Autoantibody Pathogenicity in a Multifocal Motor Neuropathy Induced Pluripotent Stem Cell–Derived Model

Oliver Harschnitz, MD,[1,2] Leonard H. van den Berg, MD, PhD,[1] Lill Eva Johansen, MSc,[2] Marc D. Jansen, DI,[1] Sandra Kling, PhD,[1] Renata Vieira de Sá, MSc,[2] Lotte Vlam, MD,[2] Wouter van Rheenen, MD,[1,2] Henk Karst, PhD,[2] Corette J. Wierenga, PhD,[3] R. Jeroen Pasterkamp, PhD,[2] and W. Ludo van der Pol, MD, PhD[1]

Objective: We investigated the pathogenicity of immunoglobulin M (IgM) anti-GM1 antibodies in serum from patients with multifocal motor neuropathy (MMN) using human induced pluripotent stem cell (iPSC)-derived motor neurons (MNs).

Methods: iPSCs were generated from fibroblasts and differentiated into MNs. We studied the binding of IgM to MNs, their complement-activating properties, and effects on structural integrity using fluorescence and electron microscopy. Live cell imaging was used to study effects of antibody binding on MNs in the presence and absence of complement.

Results: IgM antibody binding to MNs was detected using sera from MMN patients with and without detectable anti-GM1 IgM antibody titers in enzyme-linked immunosorbent assay, but not with sera from (disease) controls. Competition and depletion experiments showed that antibodies specifically bound to GM1 on iPSC-derived MNs. Binding of these antibodies disrupted calcium homeostasis by both complement-dependent and complement-independent pathways. MNs showed marked axonal damage after complement activation, and reduced antibody pathogenicity following treatment with immunoglobulin preparations.

Interpretation: Our data provide evidence for the pathogenicity of anti-GM1 IgM antibodies in MMN patients and link their presence to the clinical characteristics of axonal damage and immunoglobulin responsiveness. This iPSC-derived disease model will facilitate diagnosis, studies on autoantibody pathogenicity, drug development, and screening in immune-mediated neuropathies.

ANN NEUROL 2016;80:71–88

Multifocal motor neuropathy (MMN) is an inflammatory peripheral neuropathy that causes progressive weakness in young and middle aged patients.[1,2] It is characterized by conduction block (CB) and often by the presence of IgM antibodies against the glycosphingolipid GM1 that is abundantly expressed in (peri)nodal regions of peripheral nerves.[1] Antibody-mediated demyelination and disruption of the structural integrity at the nodes of Ranvier may underlie MMN, but the pathogenic mechanisms have not been established due to a lack of relevant in vitro or animal models for this disease.[2] Treatment response to intravenous immunoglobulins is often incomplete, and accumulating axonal damage eventually results in moderate to severe disability in a significant proportion of patients with MMN.[2–4] The development of more effective treatment strategies for MMN depends on a better understanding of the underlying etiology, and the development of disease models that recapitulate important disease characteristics is therefore crucial.

View this article online at wileyonlinelibrary.com. DOI: 10.1002/ana.24680

Received Aug 26, 2015, and in revised form Apr 25, 2016. Accepted for publication Apr 25, 2016.

Address correspondence to Dr van den Berg, Department of Neurology, Brain Center Rudolf Magnus, University Medical Center Utrecht, Heidelberglaan 100, 3584 CX, Utrecht, the Netherlands. E-mail address: l.h.vandenberg@umcutrecht.nl

From the [1]Department of Neurology and Neurosurgery, University Medical Center Utrecht, Brain Center Rudolf Magnus; [2]Department of Translational Neuroscience, University Medical Center Utrecht, Brain Center Rudolf Magnus; and [3]Division of Cell Biology, Department of Biology, Faculty of Science, Utrecht University, Utrecht, the Netherlands

The presence of anti-GM1 immunoglobulin M (IgM) antibodies was reported in the earliest descriptions of MMN, and their complement-activating properties in vitro were documented more recently.[5–9] However, their pathogenicity to nerves remains to be established. Because CB and anti-GM1 specificity of IgG autoantibodies are also characteristics of acute motor axonal neuropathy, a pathogenic model of MMN in which anti-GM1 IgM antibodies cause complement-mediated structural changes at the nodes of Ranvier has been proposed. IgM antibody binding to GM1 could additionally disrupt several of its important physiological functions, for example as receptor modulator of neurotrophic factors that control neuritogenesis and apoptosis, or as part of multimolecular assemblies in lipid rafts in membrane signaling and trafficking.[10–13]

Human induced pluripotent stem cell (iPSC)-derived motor neurons (MNs) have been used successfully to model amyotrophic lateral sclerosis (ALS) and have led to the identification of early functional phenotypes and downstream disease pathways.[14–19] In the present study, iPSC-derived MNs helped to establish the pathogenicity of IgM anti-GM1 antibodies via both complement-dependent and complement-independent pathways. Antibody binding was also present in iPSC-derived sensory neurons (SNs), but did not lead to structural damage. These results demonstrate that iPSC-derived MNs are a powerful tool for studying the pathophysiology of MMN and possibly other antibody-mediated inflammatory neuropathies.

Subjects and Methods

Patients and Controls

Serum was obtained from 39 patients with MMN, 20 gender- and age-matched (±5 years) healthy controls, and 21 ALS disease controls and stored at −80°C. All participants were Caucasian and of Dutch descent. Patients fulfilled the diagnostic consensus criteria for MMN and revised El Escorial for ALS .[20,21] Anti-GM1 IgM antibody titers had previously been determined by enzyme-linked immunosorbent assay (ELISA).[22] Healthy controls consisted of persons without systemic infections, autoimmune diseases, or neurological diseases. Ethical approval was granted by the Medical Ethical Committee of the University Medical Center Utrecht, and all subjects gave written informed consent.

Generation of iPSCs

Skin biopsy samples were obtained from 3 healthy individuals under a protocol approved by the institutional review board. Human fibroblasts were maintained in culture in mouse embryonic fibroblast (MEF) medium containing DMEM GlutaMAX (Life Technologies, Carlsbad, CA), 10% fetal bovine serum (Sigma, St Louis, MO), and 1% penicillin/streptomycin (Life Technologies). Cells were cultured at 37°C with 5% CO_2. Cellular reprogramming was performed on low-passage human fibroblasts (<P5). To generate iPSCs, human fibroblasts were plated at a density of 10,000 cells per well in a 6-well dish and cultured for 24 hours. Subsequently, viral transduction was performed with a lentiviral vector mixture containing MEF medium, 4mg/ml hexadimethrine bromide (Sigma), and lentiviral vector expressing Oct4, Klf4, Sox2, and c-Myc.[23] Following a 24-hour incubation, cells were washed 3 times with phosphate-buffered saline (PBS) and cultured for 5 days in MEF medium. Thereafter, cells were incubated with Trypsin-EDTA (Life Technologies) and transferred to a 10cm dish, precoated with 0.1% gelatin, containing a confluent layer of irradiated MEFs in MEF medium. Culture medium was replaced by human embryonic stem cell (huES) medium containing DMEM-F12 (Life Technologies), knockout serum replacement (Life Technologies), penicillin/streptomycin (Life Technologies), L-glutamine (Life Technologies), nonessential amino acids (Life Technologies), β-mercaptoethanol (Merck Millipore, Billerica, MA), and 20ng/ml recombinant human fibroblast growth factor-basic (Life Technologies). Colonies of iPSCs were manually picked after 3 to 6 weeks for further expansion and characterization. iPSCs were maintained in huES medium, cryopreserved after 4 to 6 passages, and stored in liquid nitrogen. iPSCs (<P40) were cultured on irradiated MEFs in huES medium and passaged manually. Feeder-free culture of iPSCs was performed on Geltrex (Life Technologies) and maintained in mTeSR1 medium (STEMCELL Technologies, Vancouver, BC, Canada). Feeder-free cultured iPSCs were passaged enzymatically using Accutase (Innovative Cell Technologies, San Diego, CA.). All cell lines were routinely (every 2 weeks) tested for mycoplasma infections.

MN Differentiation

MN differentiation (illustrated in Fig 1A) was performed using a modified version of previously established protocols.[24,25] In short, embryoid body (EB) formation was accomplished through a standardized microwell assay.[26,27] iPSCs were detached and seeded in microwells at a density of 150 cells/microwell in huES medium supplemented with 10μM Y-27632 (Axon Medchem, Groningen, the Netherlands) to minimize cell death. After 48 hours, medium was changed from huES medium to neural induction medium (NIM) containing DMEM-F12 (Life Technologies), penicillin/streptomycin (Life Technologies), L-glutamine (Life Technologies), nonessential amino acids (Life Technologies), N2 supplement (Life Technologies), and 20% D-glucose (Sigma). For neuralization of EBs, dual-SMAD signaling was inhibited between days 1 and 5 using 10μM SB431542 (Axon Medchem) and 0.2μM LDN193189 (Miltenyi Biotec, Bergisch Gladbach, Germany), respectively. During the first 4 days, 10μM Y-27632 (Axon Medchem) was used to inhibit cell death. EBs were carefully flushed out of the microwells using NIM containing 10μM SB431542 (Axon Medchem), 0.2μM LDN193189 (Miltenyi Biotec), 1μM retinoic acid (Sigma), and 10ng/ml brain-derived neurotrophic factor (BDNF; R&D Systems, Minneapolis, MN)

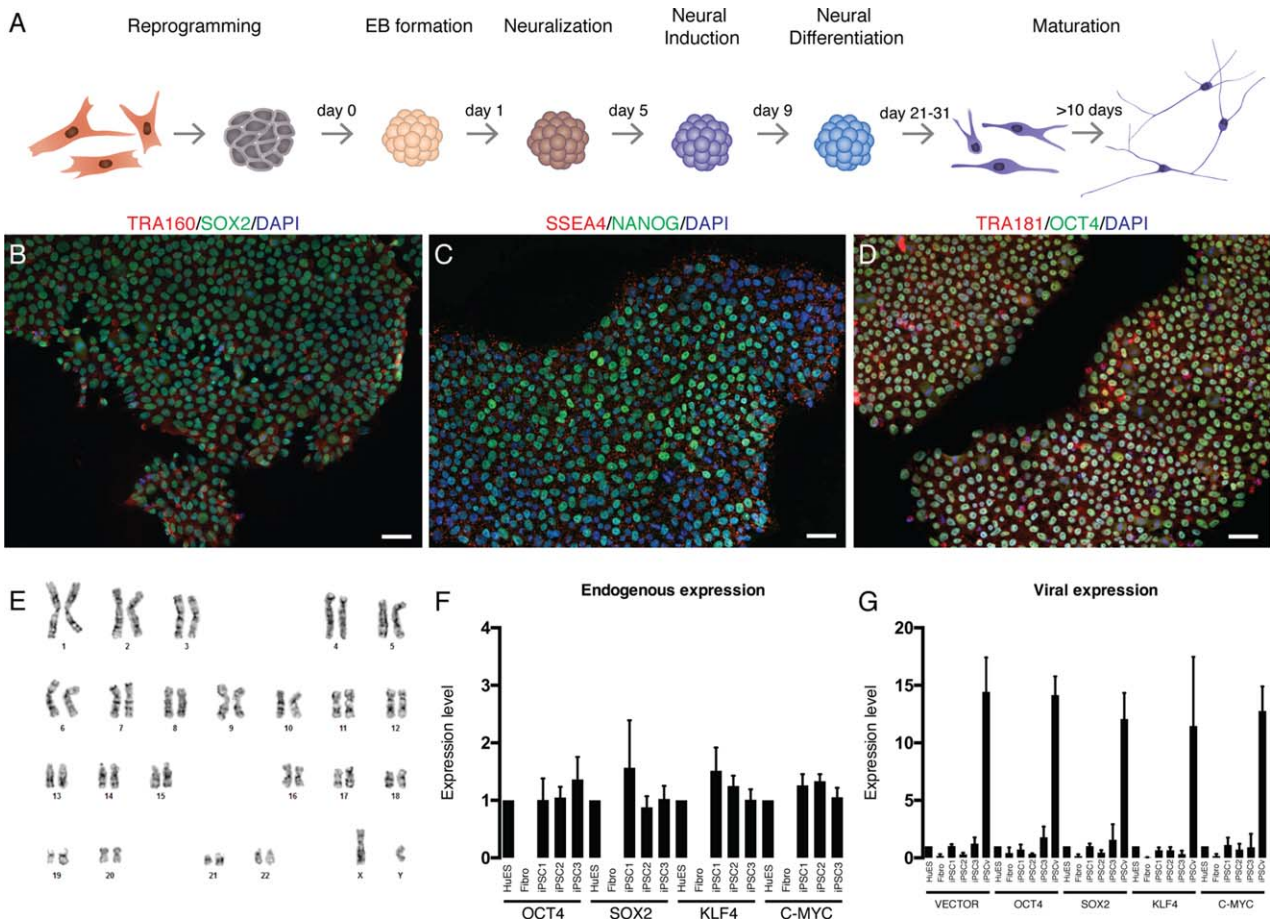

FIGURE 1: Characterization of human induced pluripotent stem cell (iPSC) lines. (A) Schematic overview of the development of motor neurons derived from human iPSCs following reprogramming from healthy control fibroblasts. (B–D) Representative images of iPSCs confirming pluripotent state by double staining for pluripotency markers TRA160 and SOX2, SSEA4 and NANOG, TRA181 and OCT4. (E) No karyotypic abnormalities were observed. A representative karyogram is depicted. (F, G) Gene expression was measured for endogenous and viral encoded transcripts. Expression for endogenous loci in all iPSC lines was similar to that of the human embryonic stem cell line HuES-2 (F). Expression of viral transcripts of OCT4, SOX2, KLF4, and c-MYC were absent in all iPSC lines. A positive control used for testing for viral transcripts was a partially reprogrammed iPSC line, in which the virus had not been silenced. Scale bars: BD, 50μm. DAPI = 4,6-diamidino-2-phenylindole; EB = embryoid body.

and transferred to a nonadherent 10cm petri dish (Greiner Bio-One, Monroe, NC). EBs were kept in suspension culture, and medium was changed every other day using NIM containing 1μM retinoic acid (Sigma), 1μM smoothened agonist (Merck Millipore), and 10ng/ml BDNF (R&D Systems). From day 16 onward, medium was changed every other day using Neurobasal differentiation medium containing Neurobasal (Life Technologies), penicillin/streptomycin (Life Technologies), L-glutamine (Life Technologies), nonessential amino acids (Life Technologies), N2 supplement (Life Technologies), B27 minus vitamin A (Life Technologies), and 20% D-glucose (Sigma) supplemented by 1μM retinoic acid (Sigma), 1μM smoothened agonist (Merck Millipore), 10ng/ml BDNF (R&D Systems), 10ng/ml glial cell line-derived neurotrophic factor (GDNF; R&D Systems), and 10 ng/ml ciliary neurotrophic factor (CNTF; R&D Systems). From days 21 to 31, EBs were dissociated using papain (Worthington Biochemical Corporation, Lakewood, NJ) and DNAse (Worthington Biochemical Corporation). Cells were resuspended in human MN medium containing Neurobasal (Life Technologies), penicillin/streptomycin (Life Technologies), L-glutamine (Life Technologies), nonessential amino acids (Life Technologies), N2 supplement (Life Technologies), and B27 minus vitamin A (Life Technologies) supplemented by 10ng/ml BDNF (R&D Systems), 10ng/ml GDNF (R&D Systems), and 10ng/ml CNTF (R&D Systems) and plated on poly-D-lysine (PDL)-laminin–coated coverslips at the required density. Coverslips with MNs were then cocultured with primary mouse glia for 2 to 3 weeks.

SN Differentiation

SN differentiation was performed by directed differentiation of iPSC lines following a previously established protocol.[28,29] In short, iPSCs were grown to 75% density, after which medium was changed to huES medium with the addition of 10μM SB431542 (Axon Medchem) and 0.2μM LDN193189 (Miltenyi Biotec) as dual-SMAD inhibition. From day 5 onward, 10μM CHIR99021 (Sigma), 10μM DAPT (Sigma), and 10μM SU5402 (Sigma) were added to the previously described

medium. Between days 8 and 10, when fully confluent, cells were passaged and plated on PDL-laminin–coated coverslips. From day 10 onward, medium was replaced with neural growth medium, containing DMEM-F12 (Life Technologies) and 10% fetal bovine serum (Sigma), supplemented by 10ng/ml BDNF (R&D Systems), 10ng/ml GDNF (R&D Systems), 10ng/ml NGF (PeproTech, Rocky Hill, NJ), 10ng/ml NT-3 (PeproTech), and 200μM ascorbic acid (Sigma).

Electrophysiological Recordings

iPSC-derived MNs were plated on 12mm coverslips following 3 weeks of differentiation and cocultured with primary mouse glia for at least 14 days. Coverslips with neuronal cultures were placed in a recording chamber, continuously perfused at room temperature (RT; 21°C) with artificial cerebrospinal fluid containing 120mM NaCl, 3.5mM KCl, 1.3mM $MgSO_4$, 1.25mM NaH_2PO_4, 2.5mM $CaCl_2$, 10mM D-glucose, and 25mM $NaHCO_3$, gassed with 95% O_2 and 5% CO_2, pH 7.4. Using an upright microscope (Axioskop; Zeiss, Oberkochen, Germany), individual MNs were visualized and selected for whole-cell current-clamp recordings. Patch pipettes for recording were produced from borosilicate glass (1.5mm outer diameter, 0.86mm inner diameter; Harvard Apparatus Limited, Holliston, MA; pipette resistance $\sim$ 4–5MΩ) on a P-97 Flaming/Brown micropipette puller (Sutter Instruments, Novato, CA) and filled with pipette solution containing 140mM K-methanesulfonate, 10mM hydroxyethylpiperazine ethanesulfonic acid (HEPES), 0.1mM ethyleneglycoltetraacetic acid, 4mM MgATP, 0.3mM NaGTP, pH 7.4, adjusted with KOH. Isolated MNs were selected for recording. Whole-cell current-clamp recordings were performed using an Axopatch 200B (Molecular Devices, Sunnyvale, CA) amplifier. The responses were filtered at 5kHz and digitized at 10kHz using Digidata 1322A (Axon Instruments, Sunnyvale, CA). All data were stored and analyzed on a personal computer using pClamp 9.0 and Clampfit 9.2 (Axon Instruments). Recordings with a series of resistance of $<$2.5 times the pipette resistance were accepted for analysis. If necessary, with a small holding current, MNs were kept at $-$65mV before the start of the current protocol. In 10 steps of 10pA with an interval of 30 seconds and duration of 500 milliseconds, the cells were depolarized to induce spike trains. Also, hyperpolarizing current steps of $-$10pA were included to study hyperpolarizing membrane properties.

Immunocytochemistry and Microscopy

Cells were fixed with 4% paraformaldehyde for 10 minutes at RT. Samples were permeabilized with 0.1% Triton X-100 (Sigma) for intracellular stainings, and subsequently blocked using 20% goat serum in 2% bovine serum albumin/PBS for 45 minutes at RT. Following a PBS wash, samples were incubated with MMN, ALS, or healthy control serum at a 1:50 dilution for 1 hour at RT. Samples were washed with PBS and subsequently incubated with indicated primary antibodies for 1 hour at RT, washed 3 times with PBS, and incubated with appropriate Alexa Fluor–labeled secondary antibodies for 1 hour at RT. Finally, cells were washed and mounted with Prolong Gold reagent with DAPI (Invitrogen, Carlsbad, CA).

The following commercial antibodies were used: rabbit anti–Oct-4A (Stem Light Pluripotency Antibody Kit; BIOKÉ, Leiden, the Netherlands), rabbit anti-Sox2 (Stem Light Pluripotency Antibody Kit, BIOKÉ), rabbit anti-Nanog (Stem Light Pluripotency Antibody Kit, BIOKÉ), mouse anti-SSEA4 (Stem Light Pluripotency Antibody Kit, BIOKÉ), mouse anti-TRA160 (Stem Light Pluripotency Antibody Kit, BIOKÉ), mouse anti-TRA181 (Stem Light Pluripotency Antibody Kit, BIOKÉ), rabbit anti–Tubulin-β3 (Sigma), mouse anti-Nestin (JM BIOCONNECT, Tilburg, the Netherlands), mouse anti-Hb9 (Developmental Studies Hybridoma Bank [DSHB], Iowa City, IA), mouse anti–Isl-1 (DSHB), goat anti-ChAT (Millipore, Billerica, MA), cholera toxin B subunit (Sigma), cholera toxin B subunit–Alexa488 conjugate (Invitrogen), goat antihuman IgM-Biotin antibody (Sigma), mouse anti-C5b-9 (Santa Cruz Biotechnology, Santa Cruz, CA), mouse anti-Brn3a (Santa Cruz Biotechnology), and rabbit anti-Peripherin (Merck Millipore). We used streptavidin-Alexa555, Alexa488, and Alexa568 secondary antibodies (Invitrogen). Other reagents used were C1q-depleted serum (CompTech, Tyler, TX), and C5-depleted serum (CompTech).

Images were acquired using either an Olympus (Tokyo, Japan) Fluoview FV1000 confocal microscope or a Zeiss Axioskop microscope followed by image analysis using ImageJ (National Institutes of Health, Bethesda, MD) software.

Live Cell Ca^{2+} Imaging and Imaging Analysis

iPSC-derived MNs were plated on 18mm round coverslips following 3 weeks of differentiation and cocultured with primary mouse glia for 14 days. Live-cell calcium imaging recordings were obtained via epifluorescence microscopy in neuronal cultures 2 weeks after plating. Prior to imaging, neuronal cultures were loaded with a Ca^{2+}-sensitive fluorescent indicator, Oregon Green BAPTA-1 (Sigma), and incubated for 50 minutes at 37°C. For imaging, cells were mounted in a recording chamber and 1ml HEPES (140mM NaCl, 5mM KCl, 2mM CaCl, 1mM MgCl, 10mM HEPES, pH 7.3) buffer was added. Cells were maintained at 37°C for the full duration of imaging experiments. All imaging used a movable live cell specimen stage of a Nikon (Tokyo, Japan) Ti microscope. Images were captured using a $\times$20 objective and μManager (University of California, San Francisco, San Francisco, CA) imaging software. Baseline measurements were obtained for 10 minutes prior to serum incubation. Serum was then added at a dilution on 1:50, after which imaging was continued for 10 minutes. Image analysis was performed using ImageJ software. Calcium signals were recorded in somata and averaged per field of view. Background fluorescence was determined in areas without cellular structures and subtracted. Largest neurons, most likely to be MNs,[19] were selected manually in ImageJ for analysis based on morphology, and their soma was selected as regions of interest (ROIs) for further measurements. All longitudinal imaging recordings were monitored to ensure ROIs did not drift off somata of selected neurons. Fluctuations in Ca^{2+} signals following serum

incubation were assessed using a Student *t* test in R (http:/r-project.org).

Scanning Electron Microscopy

Neuronal cultures where incubated with PBS, human pooled serum (HPS), heat-inactivated MMN serum, MMN serum, or heat-inactivated MMN serum with HPS as an external complement source. Incubation was performed at 37°C for 15 or 30 minutes. Samples were fixed using 4% paraformaldehyde as described above. Serial dehydration was achieved by consecutive incubation steps in 12.5% EtOH in PBS, 25% EtOH in PBS, 50% EtOH in PBS, 75% EtOH in H_2O, 90% EtOH in H_2O, 100% EtOH, followed by incubation in 50% EtOH/50% hexamethyldisilazane (HDMS) and finally 100% HDMS. Samples were mounted onto aluminum specimen mounts (Agar Scientific, Stansted, UK), followed by coating with 1nm gold using a Q150R S Rotary-Pumped Sputter Coater (Quorum Technologies, Lewes, UK). Samples were examined with a Nova NanoSEM 200 scanning electron microscope (FEI, Hillsboro, OR) operated with an accelerated voltage of 10kV at a magnification of ×7,500 using a Phenom Pro desktop scanning electron microscope and Pro Suite software (Phenom-World, Eindhoven, the Netherlands).

Statistical Analysis

Colocalization of GM1 and anti-GM1 IgM in human iPSC-derived MNs was analyzed using the JACoP plugin for ImageJ. Costes automatic thresholding was applied to determine the optimal threshold for each channel. Linear regression analysis of quantified colocalization of serum incubation experiments was performed to establish correlation between ant-GM1 titer and correlation coefficient. Statistical analyses were performed in R. Fluctuations in Ca^{2+} signals following serum incubation were assessed using a Student *t* test in R. Continuous variables with normal distribution were compared using 2-tailed Student *t* test or analysis of variance.

Results

Generation of iPSCs and Functional MNs That Express GM1 Gangliosides

We derived fibroblasts from 3 healthy controls, and reprogrammed them using a lentiviral vector encoding Klf4, Sox2, Oct4, and c-Myc.[23,30] iPSC lines were expanded and extensively characterized using a range of standardized pluripotency assays (see Fig 1). Reverse transcription polymerase chain reaction was performed to ensure that viral expression of transcription factors was silenced in all selected iPSC clones. Karyotyping of all iPSC lines showed they harbored no chromosomal aberrations. iPSC lines were tested for differentiation potential by spontaneous differentiation assays, showing competent differentiation into mesoderm, endoderm, and ectoderm (data not shown). We differentiated iPSCs into MNs expressing Nestin, Tubulin-βIII, and ISL1 using a modestly modified version of a previously described protocol (Fig 2).[24,25] Quantification of ISL1-positive cells was performed to determine the proportion of MNs. MN differentiation of each line (n = 3) was performed at least 3 times. Electrophysiological recordings of MNs showed in vitro maturation. Electrophysiological analyses to determine their maturity were obtained from the largest neurons by whole-cell patch clamp and current-clamp techniques.[19] In addition, MN cultures formed functionally active networks, as determined by live-cell calcium imaging. Because the validity of iPSC-derived MNs as a disease model for MMN depends on MN expression of GM1, we further characterized iPSC-derived MNs using anti-B subunit cholera toxin, a high-affinity ligand for GM1.[31] iPSC-derived MNs showed abundant expression of GM1 gangliosides over most neurites, overlapping with expression of Tubulin-βIII. Collectively, these results demonstrate that human iPSC-derived MNs exhibit functional properties of differentiated MNs and express the nerve constituents required to function as a valid in vitro disease model for MMN and other inflammatory neuropathies.

IgM Anti-GM1 Antibodies Specifically Bind GM1 on Human MNs

To determine the pathogenicity of IgM anti-GM1 antibodies, we first investigated their binding to human MNs in vitro (for schematic overview, see Fig 3). Neurons differentiated from all 3 iPSC lines were incubated with healthy control serum (n = 20), disease control (ALS) serum (n = 21), or MMN patient serum (n = 39; all sera diluted 1:50), prior to staining for GM1 and anti-GM1 antibodies. Incubation with healthy control or disease control serum did not lead to specific staining for IgM antibodies (for clinical characteristics of patients and controls, see Table). In contrast, incubation with MMN patient serum resulted in significant anti-GM1 staining over neurites, which colocalized with cholera toxin staining. To quantify colocalization between IgM antibody and GM1 ganglioside staining, we performed image correlation analysis. Weak correlation was found following incubation with healthy control serum ($R^2 = 0.238$) or disease control serum ($R^2 = 0.315$), and these groups did not differ statistically ($p = 0.670$). In contrast, incubation with MMN serum resulted in increased colocalization values ($R^2 = 0.407$, $p = 1.41 \times 10^{-5}$). Further analysis revealed that MMN patients, negative for anti-GM1 antibodies (MMN_{neg}) as tested by ELISA, also showed significantly increased colocalization when compared to healthy controls ($R^2 = 0.359$, $p = 0.0171$). Analysis using sera of MMN patients with a range of IgM anti-GM1 antibody titers demonstrated that IgM

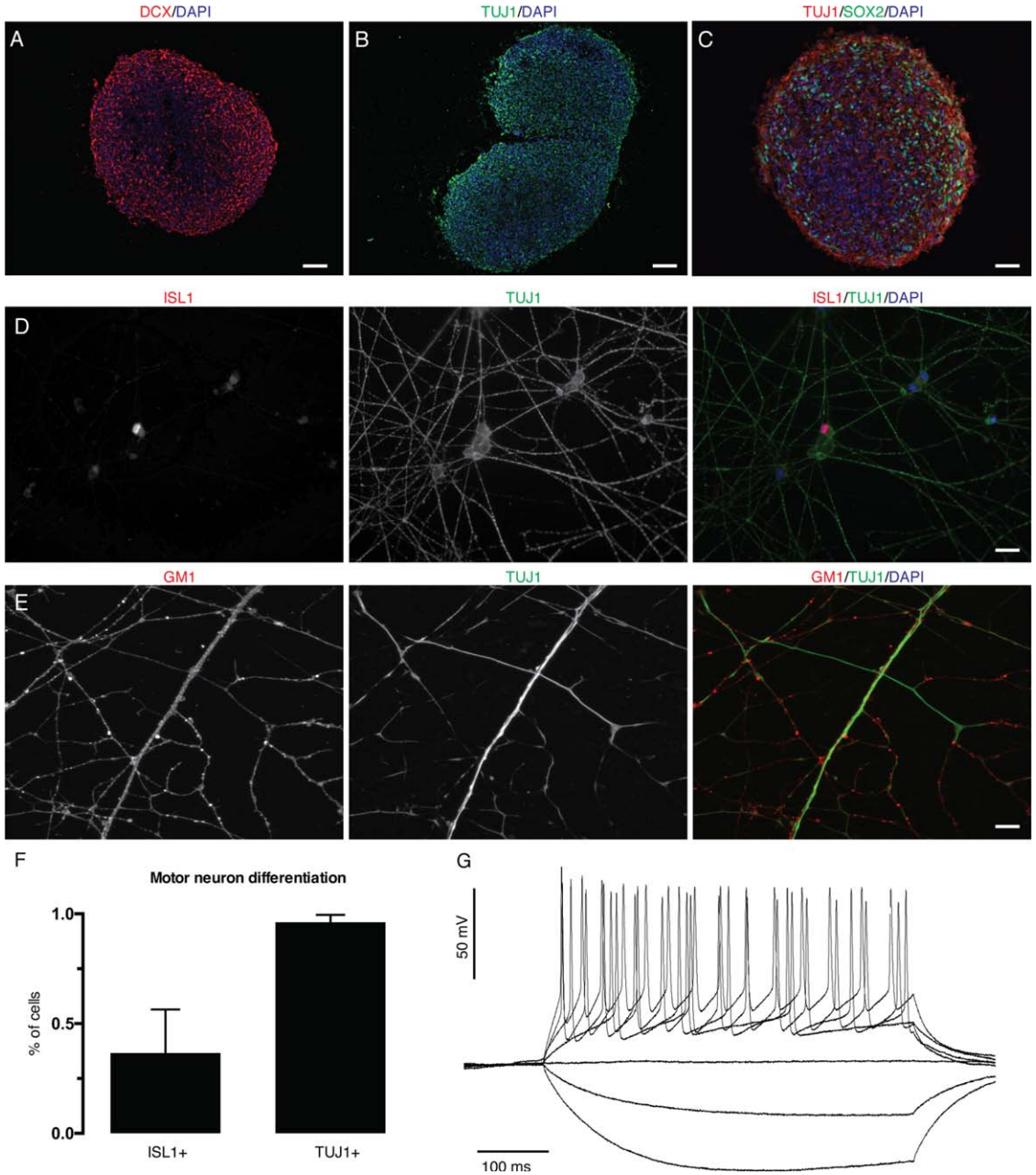

FIGURE 2: Human induced pluripotent stem cell (iPSC)-derived motor neurons (MNs) as a model for multifocal motor neuropathy. (A–C) Representative images of human iPSC-derived embryoid body following 14 days of differentiation stained for neuronal marker DCX, Tubulin-β3 (TUJ1), and SOX2 respectively. (D, E) Immunofluorescent staining of iPSC-derived MNs cultured for 14 days following 21 days of differentiation and stained for TUJ1, ISL1, and GM1. (F) Quantification of ISL1$^+$ and TUJ1$^+$ neurons at day 14 of culture. (G) Current-clamp recording following in vitro maturation of iPSC-derived MNs following current injections. MNs were capable of firing repetitive action potentials. Scale bars: A–C, 50μm; D, 100μm; E, 200μm. All results are representative of all 3 iPSC lines, with each cell line being differentiated at least 3 times. DAPI = 4,6-diamidino-2-phenylindole.

binding to neurites occurred in a titer-dependent manner ($p = 8.54 \times 10^{-6}$).

Next we assessed whether binding of IgM antibodies to human MNs was GM1-specific. First, we examined whether incubation with excess amounts of soluble unlabeled cholera toxin interfered with binding of IgM antibodies from MMN sera. Preincubation with 25μg/ml, 50μg/ml, or 100μg/ml cholera toxin efficiently prevented anti-GM1 antibodies from binding to neurons, suggesting competition of binding between cholera toxin and anti-GM1 antibodies to GM1 gangliosides (Fig 4). The use of anti-GM1 antibody-depleted serum, by serial incubation of serum with GM1-coated ELISA plates, resulted in a strong decrease in antibody binding, when

compared to nondepleted MMN serum. Interestingly, serum from MMN_{neg} patients that showed positive staining for IgM antibodies in our original experiment showed an equally reduced signal following anti-GM1 depletion compared to serum from MMN patients positive for anti-GM1 antibodies.

Our results, showing competition between cholera toxin binding and anti-GM1 binding, together with

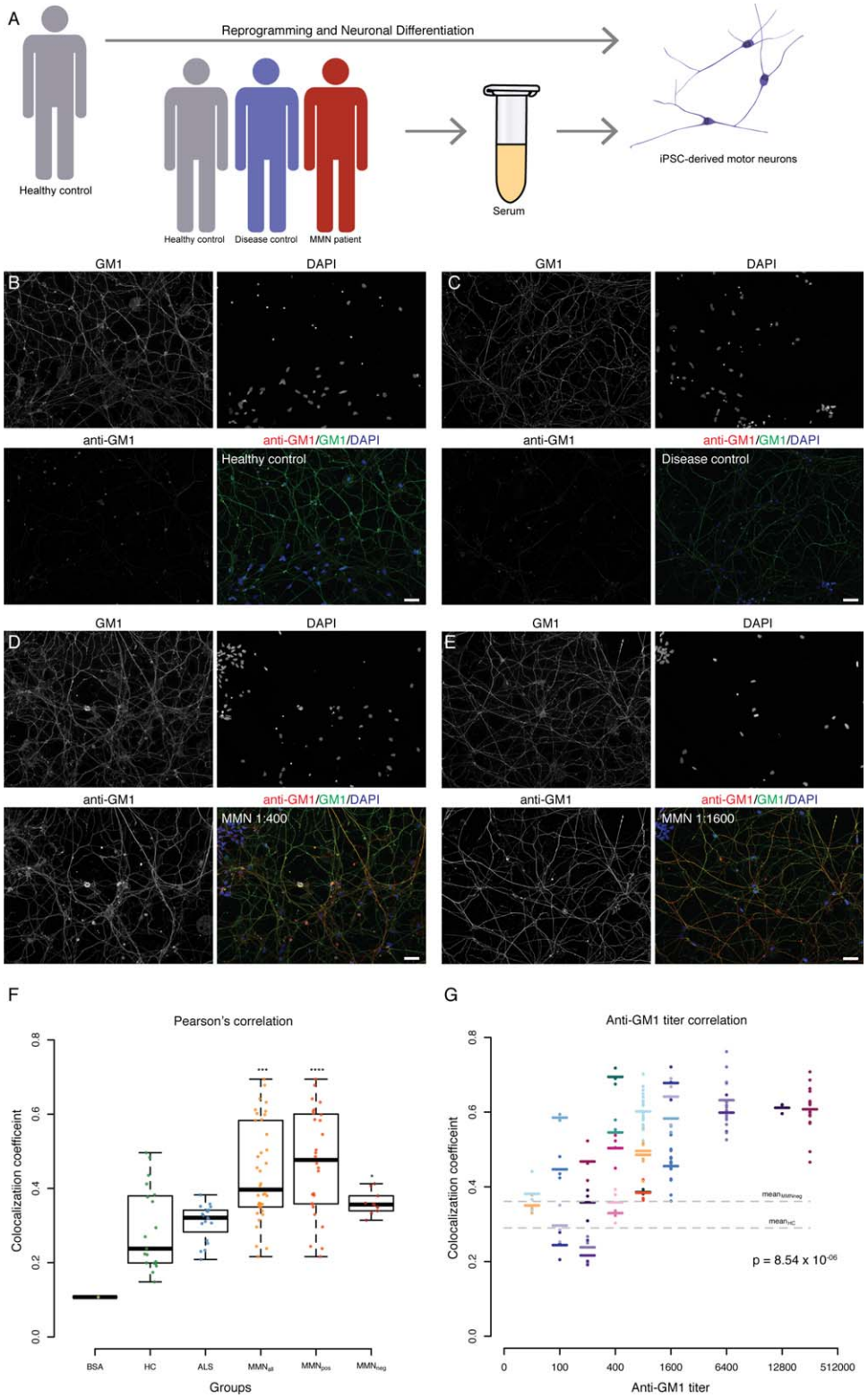

FIGURE 3.

TABLE . Demographics and Clinical Characteristics of Patients and Controls

Characteristic	Control	MMN	ALS
No.	20	39	21
Gender, male	12 (60%)	25 (64%)	14 (67%)
Age at onset, yr	42.2	39.3	53.8
Site of onset			
Bulbar	N/A	0	7
Cervical	N/A	25	9
Thoracic	N/A	0	0
Lumbar	N/A	14	5
Death within 4 years of onset	N/A	0	8
Conduction block			
Definite	N/A	33	0
Probable	N/A	6	0
Axonal loss present	N/A	34	21
IgM antibody titers > 400	0	17	0
IgM antibody titers = 0	20	10	20

ALS = amyotrophic lateral sclerosis; IgM = immunoglobulin M; MMN = multifocal motor neuropathy; N/A = not applicable.

reduced binding following antibody depletion, provide evidence that IgM anti-GM1 antibodies present in serum of MMN patients bind GM1 gangliosides in a highly specific manner. Furthermore, serum of MMN patients who are negative for anti-GM1 antibodies on ELISA assay show a similar reduction in IgM staining following anti-GM1 antibody depletion.

IgM Anti-GM1 Antibody Binding Activates Complement

Complement-activating potential of IgM anti-GM1 antibodies is an important characteristic of pathogenicity.[3,7,8,32,33] To test whether IgM anti-GM1 antibodies, after binding to neurons, activate complement and trigger complement deposition on human MNs, we incubated neurons with heat-inactivated patient serum (to inactivate complement) and HPS, which functioned as an external complement source. Following serum incubation, we determined formation of membrane attack complex (MAC), end product of the complement activation cascade. MAC deposition was clearly visible on MNs following incubation with MMN serum (Fig 5). In contrast, complement activation was never seen following incubation with HPS alone. Similarly, no MAC deposition was found in

FIGURE 3: Immunoglobulin M antibodies bind to human motor neurons. (A) Schematic overview of serum experiments, depicting motor neuron differentiation of induced pluripotent stem cell (iPSC) lines derived from healthy controls, and serum experiments using serum from healthy controls, disease (amyotrophic lateral sclerosis [ALS]) controls, and multifocal motor neuropathy (MMN) patients, respectively. (B–E) Representative images of iPSC-derived motor neurons from 3 healthy controls cocultured with primary mouse glia for 10 to 12 days and double stained for cholera toxin (green) and anti-GM1 (red). Prior to immunostaining, motor neurons were incubated with either healthy control sera (B), ALS sera (C), or MMN sera (D, E). Immunofluorescent staining of iPSC-derived motor neurons shows binding of anti-GM1 antibodies following MMN serum incubation. (F) Quantification of colocalization between anti-GM1 staining and GM1 staining using Pearson coefficient for at least 3 independent images per serum sample. Each dot represents the average correlation coefficient from a single serum sample (mean ± standard error of the mean [SEM]). Different experimental groups were bovine serum albumin (BSA; negative control group, n = 1), healthy controls (HC; n = 20), ALS (disease control group, n = 21), MMN_{all} (MMN patients, n = 39), MMN_{pos} (MMN patients with anti-GM1 antibodies as tested per enzyme-linked immunosorbent assay [ELISA], n = 31), and MMN_{neg} (MMN patients without anti-GM1 antibodies as tested per ELISA, n = 8). Student *t* test: *$p < 0.05$, ***$p < 0.001$; ****$p < 0.0001$. Data are presented as mean values ± SEM. (G) Linear regression analysis of quantified colocalization of serum incubation experiments of MMN patients with anti-GM1 antibodies (n = 39) shows positive correlation between ant-GM1 titer and correlation coefficient, $p = 8.54 \times 10^{-6}$. Each serum sample is color coded, with dots representing independent images (n = 3), and horizontal lines representing the mean correlation coefficient for each sample. Data are presented as mean values ± SEM. Scale bars, 50μm. DAPI = 4,6-diamidino-2-phenylindole.

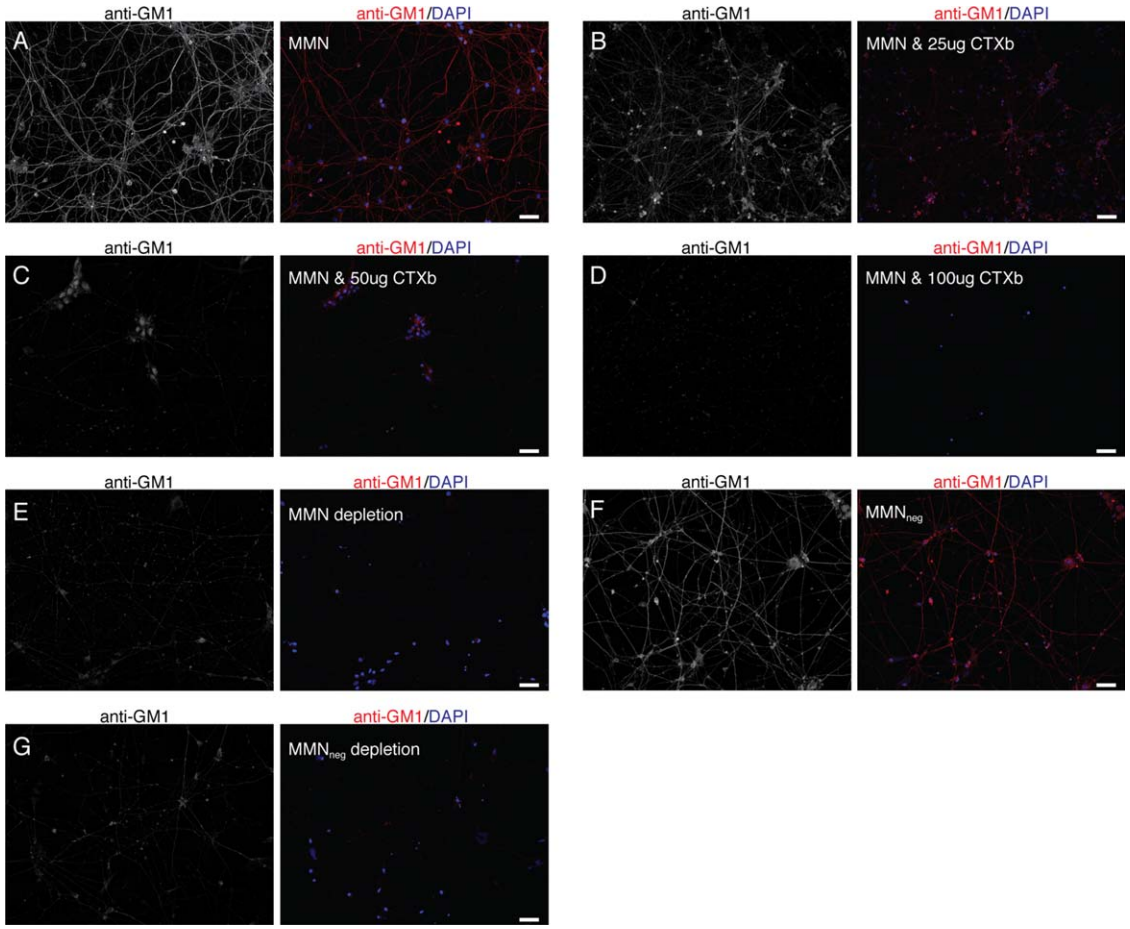

FIGURE 4: Anti-GM1 immunoglobulin M (IgM) antibody binding to human motor neurons is specific. (A–D) Coincubation with soluble unlabeled cholera toxin elicits competition and reduction of anti-GM1 IgM antibody binding. Representative images show induced pluripotent stem cell (iPSC)-derived motor neurons cocultured with primary mouse glia for 12 to 14 days and stained for anti-GM1 (red). Neuronal cultures were incubated with multifocal motor neuropathy (MMN) patient serum. (B–D) Samples were incubated with 25μg, 50μg, and 100μg of soluble unlabeled cholera toxin (CTXb), respectively, prior to MMN patient serum incubation. (E) Antibody depletion of MMN serum reduces anti-GM1 IgM antibody binding to human motor neurons. Representative images show iPSC-derived MNs cocultured with primary mouse glia for 12 to 14 days and stained for anti-GM1 (red). Neuronal cultures were incubated with GM1 antibody-depleted MMN patient serum. (F, G) Antibody depletion of MMN_{neg} serum reduces anti-GM1 IgM antibody binding to motor neurons in a similar fashion as with MMN_{pos} serum. Images were acquired at ×20 original magnification. Scale bars, 50μm. All results are representative of at least 3 independent experiments using all 3 iPSC lines. DAPI = 4,6-diamidino-2-phenylindole.

neurons incubated with either C1q-deficient serum or C5b-deficient serum as an external complement source. Although addition of immunoglobulin preparations resulted in a moderate reduction in binding of MAC, it did not prevent MAC deposition. Competition experiments using excess amounts of soluble unlabeled cholera toxin resulted in a slight reduction in binding of MAC (together with an expected reduction in GM1 staining, as seen in Fig 5F). These results demonstrate that IgM anti-GM1 antibodies are capable of activating the classical pathway of complement following binding to human MNs. Activation of the classical complement pathway persists despite immunoglobulin application or reduced binding of anti-GM1 antibodies following competition experiments.

MNs Exhibit Dysregulation of Calcium Homeostasis following Serum Incubation

As gangliosides play a role in cellular calcium levels and calcium-dependent signaling, we next used live-cell calcium imaging to determine effects of MMN serum incubation on calcium homeostasis.[34] HPS was used in parallel with MMN and heat-inactivated MMN sera. Ca^{2+} signals were slightly elevated after addition of HPS, but quickly returned to baseline. A significantly higher increase in Ca^{2+} signal was observed following MMN serum application (active MMN serum $p = 1.46 \times 10^{-6}$, and heat-inactivated MMN serum $p = 8.8 \times 10^{-8}$; Fig 6). Whereas Ca^{2+} levels in neurons incubated with heat-inactivated MMN serum returned to HPS-level within 3 minutes, Ca^{2+} levels in neurons incubated

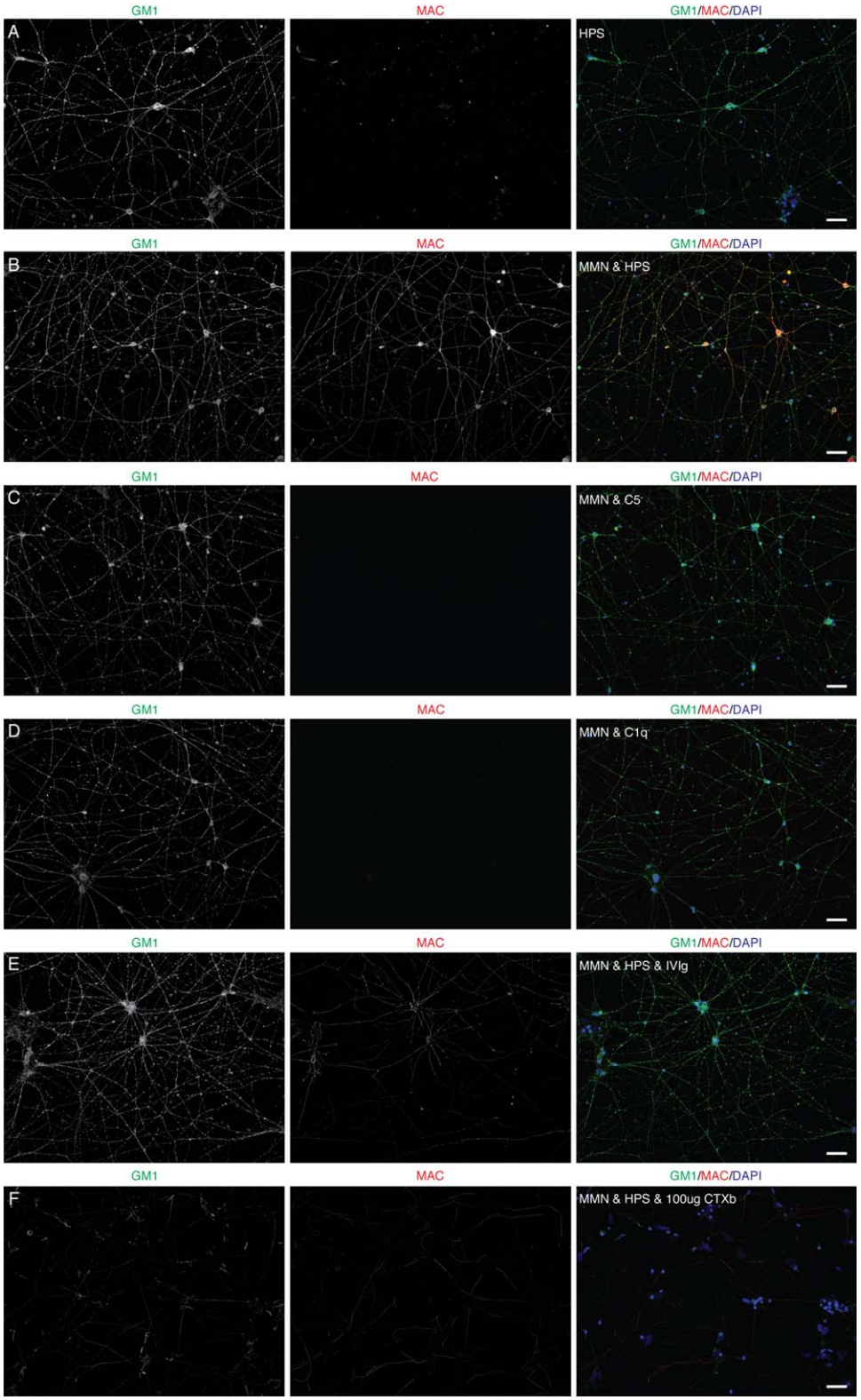

FIGURE 5: Immunoglobulin M anti-GM1 antibodies activate complement. Representative images show induced pluripotent stem cell–derived motor neurons cocultured with primary mouse glia for 12 to 14 days and stained for anti-GM1 (red) and membrane attack complex (MAC, green). Neuronal cultures were incubated with either (A) human pooled serum (HPS) or (B–D) multifocal motor neuropathy (MMN) serum lacking complement and an external complement source prior to immunostaining. External complement source was either HPS (B), C5-deficient serum (C), or C1q-deficient serum (D). (E) Preincubation of MMN serum with intravenous immunoglobulins (IVIg) reduced but did not prevent MAC deposition. (F) Competition between MMN serum and unlabeled soluble unlabeled cholera toxin (CTXb) reduced but did not prevent MAC deposition. Scale bars, 50μm. All results are representative of at least 3 independent experiments. DAPI = 4,6-diamidino-2-phenylindole.

with MMN serum with active complement remained elevated throughout the imaging period (10 minutes in total). Coincubation of MMN serum with an anti-C1q antibody as complement inhibitor prevented Ca^{2+} influx. In addition to changes in calcium levels, we observed a significant number of neurons showing morphological

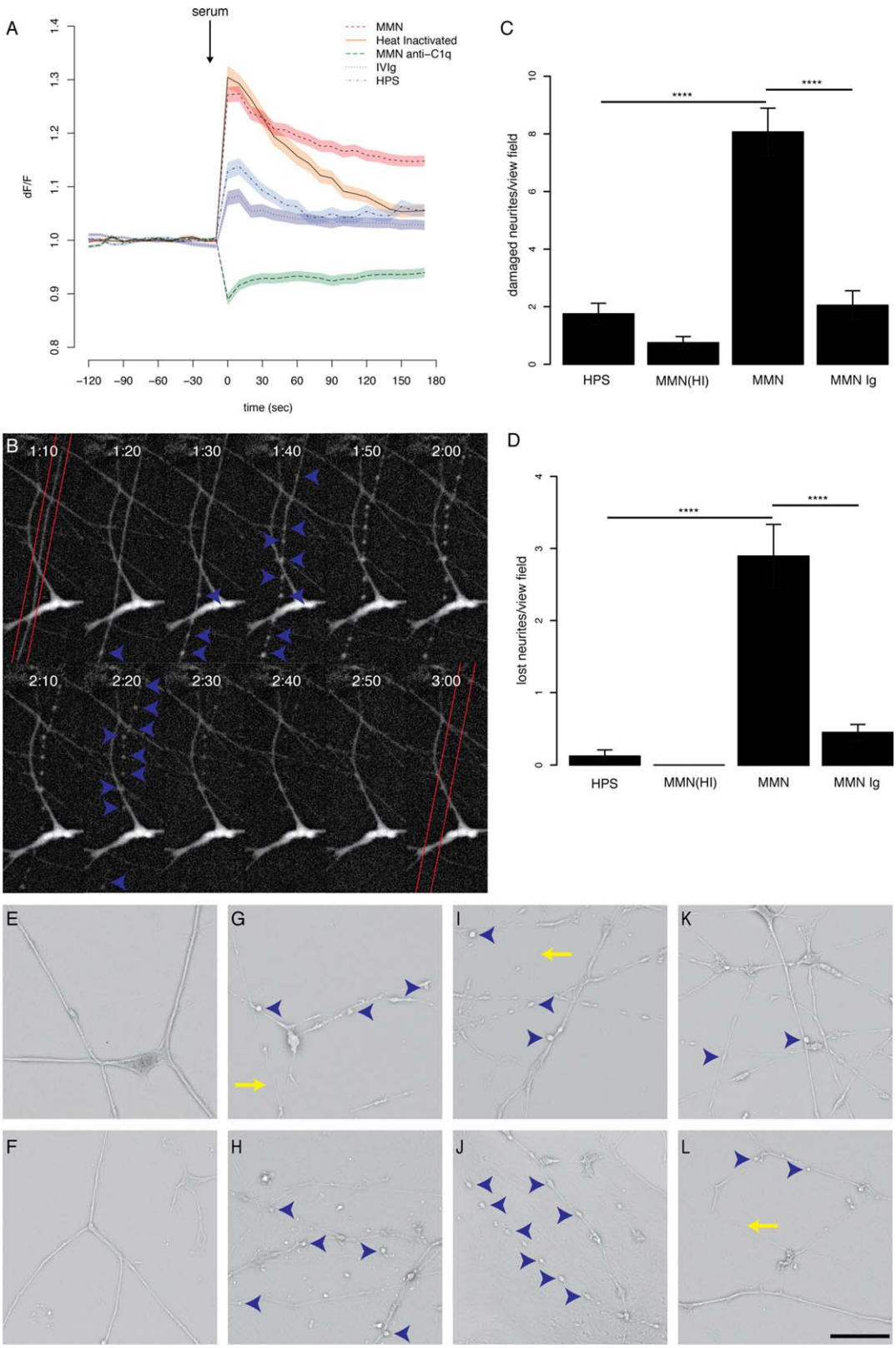

FIGURE 6.

changes resembling neurite degeneration during serum incubation. Neurons developed clear focal swelling over the length of neurites, followed by irreversible neuronal degeneration and death, reflected in a loss of fluorescent signal (eg, loss of calcium signal). To quantify these morphological changes, we counted neurites that developed clear focal swellings and neurites that completely disintegrated during the imaging period per field of view. Neuronal cultures incubated with control serum rarely showed neurite loss, and only a small number of neurites exhibited structural damage. In contrast, many neurites showed damage or complete disintegration following incubation with MMN serum (neurite damage $p = 3.4 \times 10^{-7}$, neurite loss $p = 1.0 \times 10^{-6}$).

In summary, MMN serum induced an effect on calcium homeostasis that was both complement-dependent and complement-independent. Furthermore, pronounced morphological damage was observed following incubation with MMN serum.

MNs Undergo Neurite Degeneration following MMN Serum Incubation

We next performed high-resolution imaging using scanning electron microscopy (EM) to correlate dynamic morphological information obtained from live-cell calcium imaging experiments with ultrastructural information. In line with our observations based on live-cell calcium imaging, incubation with HPS or heat-inactivated MMN serum had no deleterious effect on neuronal cultures (see Fig 6). In contrast, incubation with MMN serum resulted in marked structural damage of neurites, with pronounced focal swelling (blue arrowheads) and subsequent loss of neurites (as observed by reduced number of neurites available for imaging per coverslip). Structural damage was time-dependent, as localized swellings (blue arrowheads), thinning of neurites (yellow arrows), and loss of neurites were all increased after 30 minutes, as compared to 15 minutes, of serum incubation. Neurons showed a further increase in structural changes and neurite loss after 45- and 60-minute serum incubation. Structural damage was also observed following incubation with heat-inactivated MMN serum in combination with HPS as an external complement source, providing additional evidence that complement activation is essential for neurite damage to occur.

Therapeutic Immunoglobulin Reverses Dysregulation of Calcium Homeostasis and Alleviates Structural Damage

Intravenous or subcutaneous administration of immunoglobulins improves strength of patients with MMN in the short term and prognosis in the long term.[2,35] We tested the effects of immunoglobulin application on calcium homeostasis and structural damage following serum incubation. We preincubated MMN serum with immunoglobulins (12.5mg/ml) for 1 hour at RT prior to incubation of neuronal cultures with serum. Live-cell imaging was then performed as described earlier, with addition of MMN serum/immunoglobulin after 10-minute baseline measurements. The pathological effects observed earlier following MMN serum incubation, including acute and long-term disruptions of calcium homeostasis and morphological changes to neurites (see Fig 6A–C), were prevented by preincubation with immunoglobulin. Scanning EM experiments showed attenuation of localized swelling and thinning of neurites; however, structural damage was not completely inhibited by immunoglobulin application (see Fig 6K, L).

FIGURE 6: Immunoglobulin M anti-GM1 antibodies disrupt calcium homeostasis, and cause structural damage and neurite loss. (A) Mean calcium responses of neurons following 1:50 serum incubation, with human pooled serum (HPS; control serum, n = 134, light blue), multifocal motor neuropathy (MMN) serum (MMN patient serum with active complement, n = 294, red), MMN HI = heat inactivated serum (MMN patient serum without complement, n = 110, orange), MMN serum and intravenous immunoglobulin (IVIg; rescue condition where MMN serum with active complement was preincubated with Ig, n = 170, dark blue), and MMN serum and anti-C1q antibody (rescue condition where MMN serum with active complement was preincubated with complement inhibitor, n = 157, green). Neurons showed significantly increased Ca^{2+} responses following MMN serum incubation when compared to HPS incubation ($p = 1.46 \times 10^{-6}$). Similar responses in Ca^{2+} fluxes were seen following incubation with MMN HI serum ($p = 8.8 \times 10^{-8}$). Calcium responses were calculated as the change in fluorescence (dF) over baseline fluorescence (F). Glare represents standard error of the mean (SEM) of at least 5 independent experiments. (B) Representative images of longitudinal imaging experiments clearly depicting both initial focal swelling (blue arrow heads) and subsequent apoptosis. Red lines signify original path of neurite. (C) Quantification of number of damaged neurites of induced pluripotent stem cell (iPSC)-derived neurons following serum incubation during longitudinal imaging experiments, 5 independent experiments, n = 16–46 fields of view examined per serum condition. Student *t* test: ****$p < 0.0001$. Data are presented as mean values ± SEM. (D) Quantification of number of neurites lost from iPSC-derived neurons following serum incubation during longitudinal imaging experiments, 5 independent experiments, n = 16–46 fields of view examined per serum condition. Student *t* test: ****$p < 0.0001$. Data are presented as mean values ± SEM. (E–L). Representative scanning electron images show iPSC-derived motor neurons following serum incubation. Neurons incubated with human pooled serum and heat-inactivated MMN sera show no signs of degeneration (E, F). Following 15-minute incubation with MMN serum with active complement (G) or MMN heat-inactivated serum with an external complement source (I), neurons show focal swelling *(blue arrowheads)* and thinning *(yellow arrows)*. Degenerative morphological changes are time-dependent (H–J), as 30-minute incubation with respective sera shows increased degenerative signs. Structural damage is significantly reduced but not fully reversed by rescue with immunoglobulins (K, L). Images were acquired at ×7,500 original magnification. Scale bar: E–L, 10μm.

Immunoglobulin incubation was efficient in alleviating calcium homeostasis dysfunction, but minor structural damage could still be observed using scanning EM. Rescue of functional and reduction of morphological phenotypes by immunoglobulins highlights the potential of the disease model for studying the mechanisms of

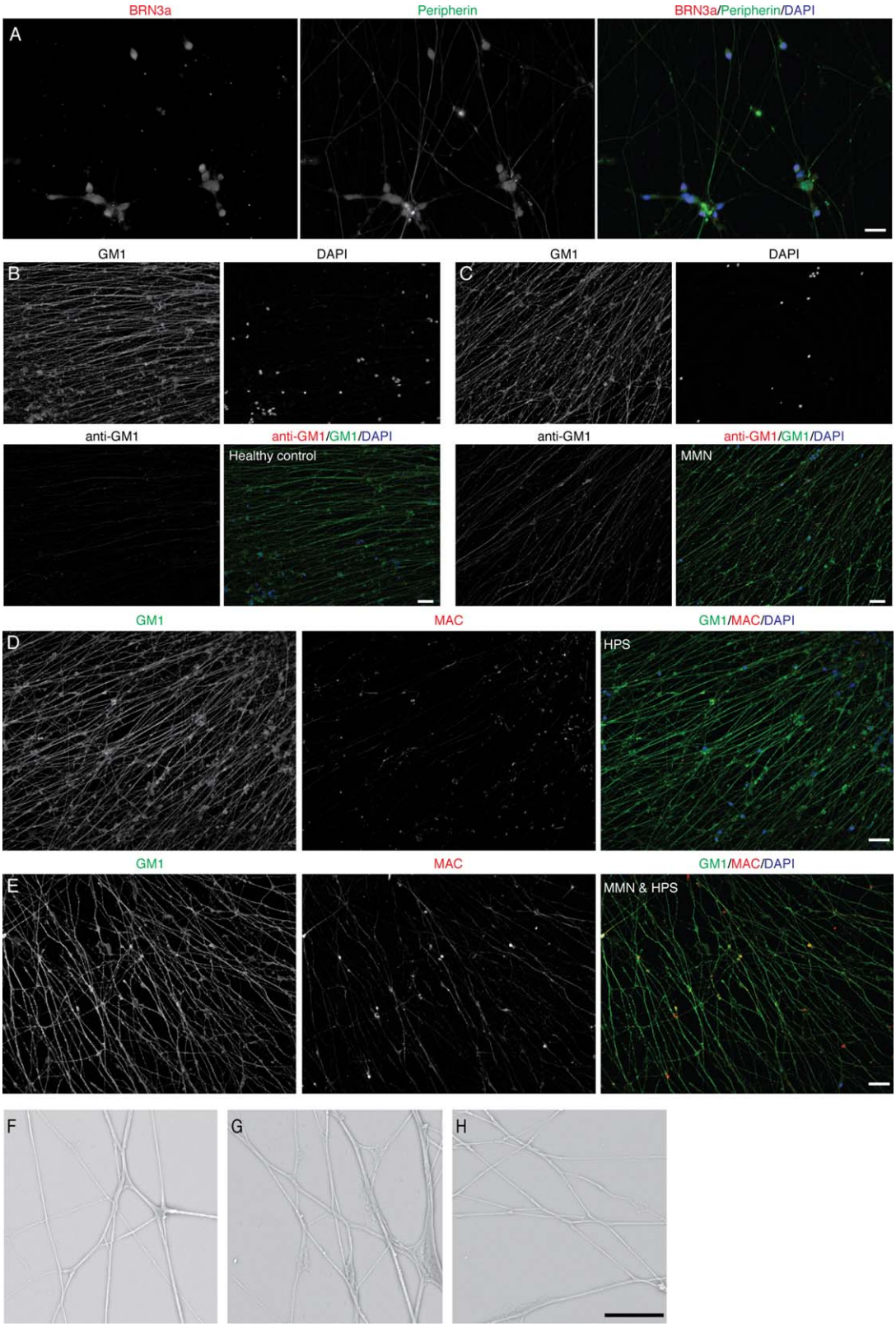

FIGURE 7.

immunoglobulin therapy and testing future potentially therapeutic compounds.

SNs Show Reduced Vulnerability to Axonal Damage Despite IgM Anti-GM1 Antibody Binding

Selective MN vulnerability is a core aspect of the MMN phenotype. To study the effects of IgM anti-GM1 antibodies to a clinically nonaffected neuronal subpopulation, we used a previously established protocol to differentiate iPSCs into BRN3a-positive and Peripherin-positive SNs (Fig 7).[28,29] Immunostaining using anti-beta subunit cholera toxin showed SNs expressed GM1 gangliosides. As with iPSC-derived MNs, we first investigated the binding of IgM anti-GM1 antibodies to iPSC-derived SNs. SNs differentiated from 2 iPSC lines were incubated with healthy control serum and MMN patient serum. In line with our MN experiments, incubation with healthy control serum did not lead to specific staining for IgM antibodies. Incubation with MMN patient serum resulted in significant anti-GM1 staining over neurites, which colocalized with cholera toxin staining in a fashion reminiscent of antibody binding to MNs.

To determine whether antibody binding to SNs leads to complement binding as previously observed in MNs, we performed serum incubation experiments in iPSC-derived SNs using heat-inactivated patient serum (to inactivate complement) and HPS, which functioned as an external complement source. MAC deposition was visible on SNs following incubation with MMN serum (see Fig 7E), but less pronounced than in previous MN experiments (see Fig 5B). Complement activation was never seen following incubation with HPS alone (see Fig 7D).

Finally, we performed high-resolution imaging using scanning EM as we did for the iPSC-derived MNs. In contrast to our observations using iPSC-derived MNs, incubation with HPS, heat-inactivated MMN serum, or MMN serum had almost no detrimental effect on SN cultures (see Fig 7F–H). In conclusion, despite anti-GM1 antibody binding and subsequent complement activation, in contrast to iPSC-derived MNs, SNs do not exhibit vulnerability to anti-GM1 mediated, complement-dependent axonal damage.

Discussion

In the present study, we describe a novel in vitro disease model for MMN using human iPSC-derived MNs and SNs. We show that IgM anti-GM1 antibodies exert several pathogenic effects that recapitulate and explain unique features of MMN, in particular the MN-specific damage to axons and the therapeutic effect of immunoglobulins (Fig 8). An important physiological function of GM1 is its role in cellular calcium homeostasis, and IgM anti-GM1 antibodies trigger intracellular dysregulation of Ca^{2+}-dependent signaling pathways in addition to complement-mediated structural damage in MNs.[34] The ability of immunoglobulins to partially rescue both functional and structural defects indicates that the model presented here might be used not only to dissect MMN disease pathways, but also to study the efficacy of novel treatment strategies.

Because anti-GM1 IgM antibodies are not found in all patients with MMN, their pathogenicity has been questioned.[2] That incubation of serum samples from MMN_{neg} patients showed enhanced IgM binding to human iPSC-derived MNs, compared to healthy and disease controls, and that these antibodies have complement-activating potential, suggest that MMN pathogenesis may be similar in most patients, and that MMN_{neg} patients harbor IgM antibodies against the same or a similar epitope. This is further underlined by the finding of reduced binding following incubation with MMN_{neg} sera that were depleted of anti-GM1 antibodies. GM1-antibody ELISA has important methodological limitations, in particular limited sensitivity.[36–38] The interaction of GM1 with other glycolipids in the axolemma of cultured MNs probably alters the antigenicity of GM1-containing complexes, thereby naturally optimizing binding and detection of anti-GM1 antibodies in patient serum.[39–42] This highlights the benefits of an in vitro humanized model system for detecting antibody binding compared to ELISA methodology.

FIGURE 7: Immunoglobulin M anti-GM1 antibodies bind to induced pluripotent stem cell (iPSC)-derived sensory neurons without causing structural damage. (A) Characterization of iPSC-derived sensory neurons by immunofluorescent staining for BRN3a and Peripherin. (B, C) Representative images of iPSC-derived sensory neurons double stained for cholera toxin (green) and anti-GM1 (red). Prior to immunostaining, sensory neurons were incubated with either healthy control sera (B), or multifocal motor neuropathy (MMN) sera (C). (D, E) Sensory neurons were incubated with either human pooled serum (HPS; D) or MMN serum lacking complement and an external complement source prior to immunostaining (E), and subsequently stained for GM1 (green) and membrane attack complex (MAC; red). (F–H) Representative scanning electron images of iPSC-derived sensory neurons following serum incubation. Neurons incubated with human pooled serum (F), heat-inactivated MMN sera (G), or MMN sera (H) show no signs of structural damage. Images were acquired at ×7,500 original magnification. DAPI = 4,6-diamidino-2-phenylindole.

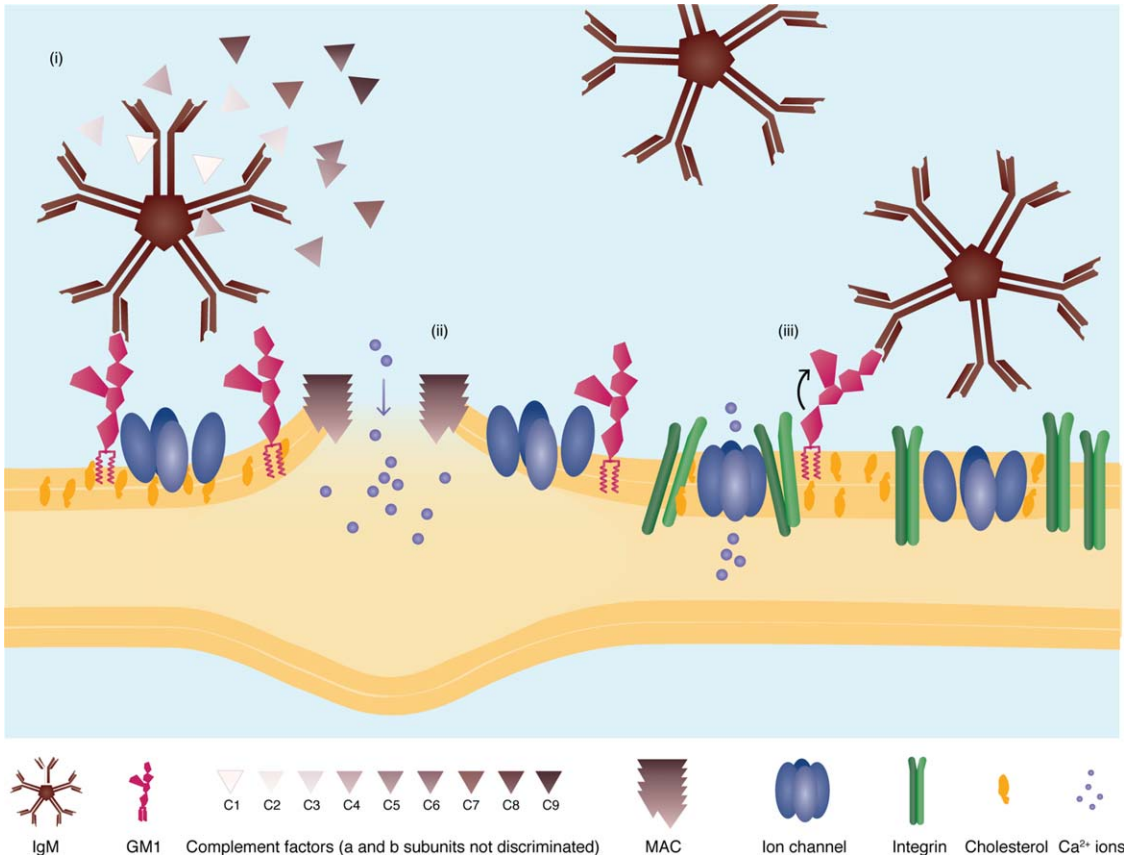

FIGURE 8: Immunoglobulin M (IgM) anti-GM1 antibodies mediate both complement-dependent and complement-independent pathogenicity to motor neurons. Model shows putative modes of anti-GM1 antibody pathogenicity, with direct IgM anti-GM1 antibody and complement-dependent pathogenic effect, to neurons. (i) Binding of IgM anti-GM1 antibodies to GM1 gangliosides results in activation of complement and deposition of the membrane attack complex (MAC). (ii) Formation and deposition of the MAC may lead to nonspecific pore formation and focal swelling, as a consequence of uncontrolled ion fluxes (eg, Ca^{2+}). Disturbance of the membrane integrity at the paranodal regions may lead to further disruption of ion channel clustering. (iii) Acute direct effects of IgM anti-GM1 antibody binding may be caused by crosslinking of GM1 gangliosides, leading to Ca^{2+} influx and subsequent activation of voltage-independent ion channels.

Pathophysiological concepts of MMN currently rely on extrapolation of data from animal models of variants of the Guillain–Barré syndrome and related disorders, which are caused by antiganglioside antibodies of the higher-affinity IgG isotype.[33,40,43,44] Previously, no effects of IgM anti-GM1 antibodies were observed in an in vitro mouse sciatic nerve model and no differences were found in complement activation between healthy control serum and MMN patient serum.[7] In our model, anti-GM1 IgM antibodies exerted multiple distinct pathogenic effects on human MNs. First, we observed complement-dependent degeneration of neurites and disruption of Ca^{2+} homeostasis following MMN sera incubation, most likely the result of nonspecific pore formation in neurons due to MAC deposition. This mechanism has been previously shown to underlie pathogenicity of antiganglioside IgG antibodies at the neuromuscular junction and the distal nodes of Ranvier in ex vivo mouse models and the in vivo rabbit model.[3,32,45–47] In these models, complement deposition caused calcium influxes that disrupted the cytoskeleton and the clustering of sodium channels. Our results suggest that lower affinity anti-GM1 IgM antibodies exert similar effects to IgG antibodies. Importantly, we observed acute Ca^{2+} disruption that was complement-independent. This has not been studied with IgG antibodies, but crosslinking of GM1 after binding of the high-affinity ligand cholera toxin initiated similar effects.[48] The pentameric structure of IgM, with its multiple binding sites, probably facilitates extensive crosslinking, but it remains to be established whether this complement-independent effect is unique for IgM.

Human iPSC-derived SNs expressed GM1, as was to be expected from previous animal and human pathology experiments. Subsequently, IgM anti-GM1 antibodies showed binding to SNs comparable to binding to MNs. Interestingly, despite activation of the classical complement pathway and MAC formation on SNs following serum incubation, this seemed to be less

pronounced compared to that seen on MNs. Even more striking was the lack of axonal damage seen following MMN serum incubation. Whether this selective vulnerability is due to a difference in epitope presentation or due to inherent differences in cell characteristics (eg, metabolic rates, electrophysiological profile) remains to be determined.

Furthermore, this iPSC-derived MN model holds the promise of enabling evaluation of the efficacy of new treatment strategies for inflammatory neuropathies. Immunoglobulins are currently the only treatment to improve muscle strength and outcome in patients with MMN.[35] In our model, application of immunoglobulins attenuated functional and morphological defects, although ultrastructural neuronal damage was not completely reversed. This finding closely mirrors the natural history of progressive axonal damage in many patients with MMN despite immunoglobulin treatment. The manner in which immunoglobulins exert their neuroprotective effect remains to be established. It has previously been shown that immunoglobulins can attenuate in vitro deposition of complement factors, as well as reduce binding of IgG antibodies, leading to a reduced deposition of MAC.[8,45] Although our model shows a reduced deposition of MAC following preincubation of serum with immunoglobulins, this reduction is modest compared to the rescue of calcium homeostasis dysfunction. Furthermore, immunoglobulins rescue complement-independent effects of IgM anti-GM1 antibodies, pointing toward a direct modulatory effect of antibody binding or anti-idiotype mechanism.[35] Our model may facilitate future studies designed to unravel neuroprotective mechanisms of action of immunoglobulins. Moreover, response to immunoglobulins differs between patients, and there are no clinical tools to predict efficacy. This model holds the promise that in vitro drug responsiveness may predict in vivo drug responsiveness and that it could be used for a personalized medicine approach or the development of novel therapeutic strategies.

Disease modeling using iPSC-derived MNs has previously been applied to studying the underlying disease mechanisms of ALS, and more recently myasthenia gravis.[14–19,49] Here we show the potential of iPSC modeling of rare inflammatory disorders. Future improvements to the currently described disease model could be the addition of a coculture with iPSC-derived Schwann cells, thereby providing in vitro myelination and formation of nodes of Ranvier.[3,50,51] Nevertheless, in its current form, the model recapitulates the progressive, irreversible axonal damage, which can in part be alleviated by immunoglobulin treatment, mimicking clinical treatment response to immunoglobulins.[52–54]

Overall, our results demonstrate that human iPSC-derived MNs represent a novel disease model for MMN, and show for the first time that IgM anti-GM1 antibodies are pathogenic to human MNs. Our ability to model MMN in vitro presents further opportunities for studying mechanisms underlying MMN and performing large-scale drug screens. Ultimately, this in vitro disease model may help to distinguish MMN patients from those with ALS, thus facilitating diagnosis and early treatment with immunoglobulins that will help to prevent permanent axonal damage. In addition, this approach can be applied more broadly to study other antibody-mediated neuropathies.

Acknowledgment

This work was supported by the Prinses Beatrix Spierfonds (WAR06-0115), the Adessium Foundation, the Netherlands Organization for Health Research and Development (ZonMW-VICI, L.H.v.d.B.; NWO-VENI, C.J.W.), the Netherlands ALS Foundation, and the European Community's Health Seventh Framework Program (grant agreement 259867).

We thank A. Schambach for sharing the polycistronic-reprogramming vector; N. Rivron for generously providing the microwell assay and helping to generate EBs; L. Rietman for her contribution to the iPSC facility and the Brain Center Rudolf Magnus iPSC facility; E. Cats, A. Tio-Gillen, and B. Jacobs for their help with anti-GM1 EILSAs; A. P. A. Hendrickx for providing assistance with scanning EM experiments, and M. van der Linde for assistance in the karyotyping of all iPSC lines. Anti-Hb9 and anti-Isl-1 antibodies were obtained from the Developmental Studies Hybridoma Bank, created by the National Institute of Child Health and Human Development of the NIH and maintained at the Department of Biology, University of Iowa, Iowa City, IA.

Author Contributions

R.J.P. and W.L.v.d.P. contributed equally to this work. O.H., M.D.J., S.K., L.E.J., R.V.d.S., L.V., W.v.R., B.M.V., H.K., and C.J.W. performed experiments and data analysis. Drafting of manuscript and figures was performed by O.H., L.H.v.d.B., R.J.P., and W.L.v.d.P. Conception and design of experiments and study were by O.H., L.H.v.d.B., R.J.P., and W.L.v.d.P.

Potential Conflicts of Interest

L.H.v.d.B., W.L.v.d.P.: travel grants, consultancy fees, Baxter International. L.H.v.d.B.: scientific advisory board, Biogen Idec, Cytokinetics.

References

1. Willison HJ, Yuki N. Peripheral neuropathies and anti-glycolipid antibodies. Brain 2002;125(pt 12):2591–2625.
2. Vlam L, van der Pol WL, Cats EA, et al. Multifocal motor neuropathy: diagnosis, pathogenesis and treatment strategies. Nat Rev Neurol 2011;8:48–58.
3. Susuki K, Rasband MN, Tohyama K, et al. Anti-GM1 antibodies cause complement-mediated disruption of sodium channel clusters in peripheral motor nerve fibers. J Neurosci 2007;27:3956–3967.
4. Kuwabara S, Yuki N. Axonal Guillain-Barré syndrome: concepts and controversies. Lancet Neurol 2013;12:1180–1188.
5. Pestronk A, Choksi R, Blume G, Lopate G. Multifocal motor neuropathy: serum IgM binding to a GM1 ganglioside-containing lipid mixture but not to GM1 alone. Neurology 1997;48:1104–1106.
6. Latov N, Hays AP, Donofrio PD, et al. Monoclonal IgM with unique specificity to gangliosides GM1 and GD1b and to lacto-N-tetraose associated with human motor neuron disease. Neurology 1988;38:763–768.
7. Paparounas K, O'Hanlon GM, O'Leary CP, et al. Anti-ganglioside antibodies can bind peripheral nerve nodes of Ranvier and activate the complement cascade without inducing acute conduction block in vitro. Brain 1999;122(pt 5):807–816.
8. Piepers S, Jansen MD, Cats EA, et al. IVIg inhibits classical pathway activity and anti-GM1 IgM-mediated complement deposition in MMN. J Neuroimmunol 2010;229:256–262.
9. Yuki N, Watanabe H, Nakajima T, Spath PJ. IVIG blocks complement deposition mediated by anti-GM1 antibodies in multifocal motor neuropathy. J Neurol Neurosurg Psychiatry 2010;82:87–91.
10. Yates AJ, Rampersaud A. Sphingolipids as receptor modulators. An overview. Ann N Y Acad Sci 1998;845:57–71.
11. Da Silva JS, Hasegawa T, Miyagi T, et al. Asymmetric membrane ganglioside sialidase activity specifies axonal fate. Nat Neurosci 2005;8:606–615.
12. Lingwood D, Simons K. Lipid rafts as a membrane-organizing principle. Science 2009;327:46–50.
13. Hall A, Róg T, Karttunen M, Vattulainen I. Role of glycolipids in lipid rafts: a view through atomistic molecular dynamics simulations with galactosylceramide. J Phys Chem B 2010;114:7797–7807.
14. Bilican B, Serio A, Barmada SJ, et al. Mutant induced pluripotent stem cell lines recapitulate aspects of TDP-43 proteinopathies and reveal cell-specific vulnerability. Proc Natl Acad Sci U S A 2012;10:5803–5808.
15. Donnelly CJ, Zhang P-W, Pham JT, et al. RNA toxicity from the ALS/FTD C9ORF72 expansion is mitigated by antisense intervention. Neuron 2013;80:415–428.
16. Wainger BJ, Kiskinis E, Mellin C, et al. Intrinsic membrane hyperexcitability of amyotrophic lateral sclerosis patient-derived motor neurons. Cell Reports 2014;7:1–11.
17. Kiskinis E, Sandoe J, Williams LA, et al. Pathways disrupted in human ALS motor neurons identified through genetic correction of mutant SOD1. Stem Cell 2014;14:781–795.
18. Barmada SJ, Serio A, Arjun A, et al. Autophagy induction enhances TDP43 turnover and survival in neuronal ALS models. Nat Chem Biol 2014;10:677–685.
19. Devlin A-C, Burr K, Borooah S, et al. Human iPSC-derived motor neurons harbouring TARDBP or C9ORF72 ALS mutations are dysfunctional despite maintaining viability. Nat Commun 2015;6:5999.
20. Van den Berg-Vos RM, Franssen H, Wokke JH, et al. Multifocal motor neuropathy: diagnostic criteria that predict the response to immunoglobulin treatment. Ann Neurol 2000;48:919–926.
21. Ludolph A, Drory V, Hardiman O, et al. A revision of the El Escorial criteria—2015. Amyotroph Lateral Scler Frontotemporal Degener 2015;16:291–292.
22. Cats EA, Jacobs BC, Yuki N, et al. Multifocal motor neuropathy: association of anti-GM1 IgM antibodies with clinical features. Neurology 2010;75:1961–1967.
23. Warlich E, Kuehle J, Cantz T, et al. Lentiviral vector design and imaging approaches to visualize the early stages of cellular reprogramming. Mol Ther 2009;19:782–789.
24. Amoroso MW, Croft GF, Williams DJ, et al. Accelerated high-yield generation of limb-innervating motor neurons from human stem cells. J Neurosci 2013;33:574–586.
25. Dimos JT, Rodolfa KT, Niakan KK, et al. Induced pluripotent stem cells generated from patients with ALS can be differentiated into motor neurons. Science 2008;321:1218–1221.
26. Rivron NC, Vrij EJ, Rouwkema J, et al. Tissue deformation spatially modulates VEGF signaling and angiogenesis. Proc Natl Acad Sci U S A 2012;109:6886–6891.
27. Rivron NC, Raiss CC, Liu J, et al. Sonic Hedgehog-activated engineered blood vessels enhance bone tissue formation. Proc Natl Acad Sci U S A 2012;109:4413–4418.
28. Qi Y, Mica Y, Lee G, et al. Combined small-molecule inhibition accelerates developmental timing and converts human pluripotent stem cells into nociceptors. Nat Biotechnol 2012;30:715–720.
29. Young GT, Gutteridge A, Fox HD, et al. Characterizing human stem cell–derived sensory neurons at the single-cell level reveals their ion channel expression and utility in pain research. Mol Ther 2014;22:1530–1543.
30. Takahashi K, Tanabe K, Ohnuki M, et al. Induction of pluripotent stem cells from adult human fibroblasts by defined factors. Cell 2007;131:861–872.
31. Holmgren J, Lönnroth I, Månsson J, Svennerholm L. Interaction of cholera toxin and membrane GM1 ganglioside of small intestine. Proc Natl Acad Sci U S A 1975;72:2520–2524.
32. O'Hanlon GM, Plomp JJ, Chakrabarti M, et al. Anti-GQ1b ganglioside antibodies mediate complement-dependent destruction of the motor nerve terminal. Brain 2001;124(pt 5):893–906.
33. Yuki N, Susuki K, Koga M, et al. Carbohydrate mimicry between human ganglioside GM1 and Campylobacter jejuni lipooligosaccharide causes Guillain-Barre syndrome. Proc Natl Acad Sci U S A 2004;101:11404–11409.
34. Ledeen RW, Wu G. Ganglioside function in calcium homeostasis and signaling. Neurochem Res 2002;27:637–647.
35. Leger JM. Immunoglobulin (Ig) in multifocal motor neuropathy (MMN): update on evidence for Ig treatment in MMN. Clin Exp Immunol 2014;178:42–44.
36. Kaida K-I, Morita D, Kanzaki M, et al. Ganglioside complexes as new target antigens in Guillain-Barré syndrome. Ann Neurol 2004;56:567–571.
37. Nobile-Orazio E, Giannotta C, Musset L, et al. Sensitivity and predictive value of anti-GM1/galactocerebroside IgM antibodies in multifocal motor neuropathy. J Neurol Neurosurg Psychiatry 2014;85:754–758.
38. Delmont E, Halstead S, Galban-Horcajo F, et al. Improving the detection of IgM antibodies against glycolipids complexes of GM1 and galactocerebroside in multifocal motor neuropathy using glycoarray and ELISA assays. J Neuroimmunol 2015;278:159–161.
39. Kusunoki S, Chiba A, Kon K, et al. N-acetylgalactosaminyl GD1a is a target molecule for serum antibody in Guillain-Barré syndrome. Ann Neurol 1994;35:570–576.
40. Kusunoki S, Kaida K-I, Ueda M. Antibodies against gangliosides and ganglioside complexes in Guillain–Barré syndrome: new aspects of research. Biochim Biophys Acta 2008;1780:441–444.

41. Willison HJ, Goodyear CS. Glycolipid antigens and autoantibodies in autoimmune neuropathies. Trends Immunol 2013;34:453–459.

42. Greenshields KN, Halstead SK, Zitman FMP, et al. The neuropathic potential of anti-GM1 autoantibodies is regulated by the local glycolipid environment in mice. J Clin Invest 2009;119:595–610.

43. Goodyear CS, O'Hanlon GM, Plomp JJ, et al. Monoclonal antibodies raised against Guillain-Barré syndrome–associated Campylobacter jejuni lipopolysaccharides react with neuronal gangliosides and paralyze muscle-nerve preparations. J Clin Invest 1999;104:697–708.

44. Halstead SK, Zitman FMP, Humphreys PD, et al. Eculizumab prevents anti-ganglioside antibody-mediated neuropathy in a murine model. Brain 2007;131:1197–1208.

45. Jacobs BC. Immunoglobulins inhibit pathophysiological effects of anti-GQ1b-positive sera at motor nerve terminals through inhibition of antibody binding. Brain 2003;126:2220–2234.

46. McGonigal R, Rowan EG, Greenshields KN, et al. Anti-GD1a antibodies activate complement and calpain to injure distal motor nodes of Ranvier in mice. Brain 2010;133:1944–1960.

47. Fewou SN, Rupp A, Nickolay LE, et al. Anti-ganglioside antibody internalization attenuates motor nerve terminal injury in a mouse model of acute motor axonal neuropathy. J Clin Invest 2012;122: 1037–1051.

48. Wu G, Lu ZH, Obukhov AG, et al. Induction of calcium influx through TRPC5 channels by cross-linking of GM1 ganglioside associated with 5.1 integrin initiates neurite outgrowth. J Neurosci 2007;27:7447–7458.

49. Steinbeck JA, Jaiswal MK, Calder EL, et al. Functional connectivity under optogenetic control allows modeling of human neuromuscular disease. Stem Cell 2015;18:134–143.

50. Liu Q, Spusta SC, Mi R, et al. Human neural crest stem cells derived from human ESCs and induced pluripotent stem cells: induction, maintenance, and differentiation into functional Schwann cells. Stem Cells Transl Med 2012;1:266–278.

51. Ma M-S, Boddeke E, Copray S. Pluripotent stem cells for Schwann cell engineering. Stem Cell Rev Rep 2014;11:205–218.

52. Van Asseldonk JTH. Axon loss is an important determinant of weakness in multifocal motor neuropathy. J Neurol Neurosurg Psychiatry 2006;77:743–747.

53. Gong Y, Tagawa Y, Lunn MPT et al. Localization of major gangliosides in the PNS: implications for immune neuropathies. Brain 2002;125:2491–2506.

54. Svennerholm L, Bostrom K, Fredman P, et al. Gangliosides and allied glycosphingolipids in human peripheral nerve and spinal cord. BBA 1994;1214:115–123.